1 Automated urban flood level detection based on flooded bus dataset using YOLOv8

2 Yanbin Qiu[a], Xudong Zhou[b],Jiaquan Wan[a,*], Tao Yang[a,c], Lvfei Zhang[a], Yuanzhuo Zhong[a],

3 Leqi Shen[a], Xinwu Ji[a]

4 [a] College of Hydrology and Water Resources, Hohai University, Nanjing 210024, China

5 [b] Institute of Hydraulics and Ocean Engineering, Ningbo University, Ningbo 315000, China

6 [c] Institute of Water Resources and Technology, Hohai University, Nanjing 210024, China

7 **Corresponding Author:**

8 Jiaquan Wan

9 College of Hydrology and Water Resources, Hohai University, Nanjing 210024, China

10 Email: 775290095@qq.com

11 **ABSTRACT**

12   Rapid and accurate acquisition of urban flood information is crucial for flood prevention, disaster

13 mitigation, and emergency management. With the development of mobile internet, crowdsourced images on

14 social media have ~~been~~ emerged as a novel and effective data source for flood information collection.

15 However, selecting appropriate targets and employing suitable methods to determine flooding level has not

16 been well investigated. You Only Look Once version 8 (YOLOv8) is a convolutional neural network-based

17 computer vision model that has been widely applied in image recognition tasks due to its end-to-end

18 architecture and high computational efficiency. This study proposes a method to assess urban flood risk

19 levels based on the submerged status of buses captured in social media images. First, a dataset containing

20 1008 images in complex scenes is constructed from social media. The images are annotated using Labelimg,

21 and expanded with a data augmentation strategy. Four YOLOv8 configurations are validated for their ability

22 to identify urban flood risk levels. The validation process involves training the models on original datasets,

23 augmented datasets, and datasets representing complex scenes. Results demonstrate that, compared to

24 traditional reference objects (e.g., cars), buses exhibit greater stability and higher accuracy in identification

25 of urban flood risk levels due to their standardized height and widespread presence as they in remain service

26 during flood events. The data augmentation strategy enhances the model's mAP50 and mAP50-95 metrics

27 by over 10% and 20%, respectively. Additionally, through comparative analysis of YOLOv8 configurations,

28 YOLOv8s demonstrates superior results and achieves an effective balance between accuracy, training time,

29 and computational resources, recommended for the identification of urban flood risk levels. This method

30 provides a reliable technical foundation for real-time flood risk assessment and emergency management of

31   urban transportation systems, with substantial potential for practical applications.

32   **Keyword: Urban Flooding; Automatic Detection; Computer Vision; Object Detection**

33   **1. Introduction**

34   With the intensification of global climate change, extreme precipitation events have increasingly

35   triggered urban pluvial flooding, severely disrupting the operation of major cities (Guan et al., 2015).

36   Concurrently, the proportion of impervious surfaces has been rising due to rapid urbanization, significantly

37   diminishing the infiltration capacity of urban landscapes and resulting in an increase in surface runoff

38   (Chaudhary et al., 2020). This has led to more frequent urban flooding incidents, imposing substantial

39   impacts and losses on urban infrastructure, transportation networks, and human wellbeing. For instance, on

40   July 20, 2021, a rare extreme rainfall event, with a record-breaking maximum hourly rainfall of 201.9 mm,

41   driven by Typhoon In-Fa struck Zhengzhou, Henan Province, China, leading to severe urban inundation that

42   resulted in 292 casualties and direct economic losses reaching 53.2 billion (Yang and Wang, 2022).

43   In the event of urban flooding, the ability to rapidly and accurately identify flood risk levels is crucial

44   for urban flood prevention, mitigation, and emergency response decision making (Fohringer et al., 2015;

45   Qian et al., 2022; Smith et al., 2017). Flood depth is widely regarded as the most representative indicator for

46   assessing the severity of flood impacts. (Betterle and Salamon, 2024). The prediction of flood depth helps

47   guide evacuation planning and resource allocation, providing decision support for emergency response and

48   thereby significantly reducing loss of life and property damage (Jiang et al., 2020; Park et al., 2021).

49   (Alizadeh Kharazi and Behzadan, 2021) pointed out that even 2.54 cm of floodwater can cause

50   approximately $27,000 in combined damages to an average one-story home. When flood depth ranges

51   between 30 to 60 cm, the risks of vehicle flotation and stalling increase substantially (Kramer et al., 2016;

52   Pregnolato et al., 2017), posing serious threats to human safety. Moreover, flood depth information on

53   various roads during rescue operations is essential as it influences resource allocation and rescue route

54   planning. For example, during Hurricane Katrina, emergency responders often requested information

55   regarding the flood extent and water depth in order to deploy appropriate vehicles for search and rescue

56   (SAR) operations and to identify the optimal routes to reach victims (Nayak and Zlatanova, 2008). In

57   addition, in Texas alone, it is estimated that approximately 75% of flood-related fatalities occur during

58   evacuation efforts via local roadways, primarily due to the lack of awareness regarding inundation depth in

59   the surrounding areas. (Alizadeh Kharazi and Behzadan, 2021). Consequently, flood depth prediction plays

60 a vital role in assessing road passability, delineating road closures, optimizing rescue logistics, and

61 prioritizing areas for emergency intervention (Jiang et al., 2020; Kundu et al., 2022) .

62   Currently, urban waterlogging monitoring primarily relies on water level gauges (Fohringer et al., 2015).

63 Although water level gauges can monitor flood depth in real-time, their deployment and maintenance are

64 costly, and the monitoring range is restricted by the installation locations, limiting their suitability for wider

65 spatial coverage (Chaudhary et al., 2020; Fohringer et al., 2015; Paul et al., 2020). Microwave remote sensing

66 methods have limitations in spatial-temporal resolution and data frequency, and are susceptible to

67 interference from clouds and obstructions, rendering them unable to determine flood depth (Chaudhary et

68 al., 2020; DeVries, 2020; Liang, 2020). An intelligent and low-cost technology capable of identifying urban

69 flood risks with extensive spatial coverage is urgently needed.

70   In recent years, with the rapid development of social media and mobile internet, the application of social

71 media data in flood monitoring and risk assessment has garnered extensive attention (Baranowski et al., 2020;

72 Kankanamge et al., 2020; Li et al., 2023; Rosser et al., 2017; Smith et al., 2017). Platforms like Weibo,

73 Twitter and Douyin provide users with channels to share flood information in real time, where user-generated

74 content (UGC) contains rich flood imagery and geolocation data, offering a novel data source for urban flood

75 level detection research (Iqbal et al., 2021). Concurrently, significant advancements have been made in

76 computer vision technology, particularly in the application of convolutional neural networks (Voulodimos

77 et al., 2018) , opening new avenues for the analysis of vast amounts of flood imagery data. Current studies

78 have attempted to use objects in social media images, such as bridges (Bhola et al., 2018), roadside barriers

79 (Jiang et al., 2019), bicycles (Chaudhary et al., 2020), traffic cones (Jiang et al., 2020), traffic signs (Alizadeh

80 Kharazi and Behzadan, 2021), water level markers (Jafari et al., 2021), and pedestrians (Li et al., 2023), as

81 reference points for flood level estimation. While specific reference objects have shown promising results

82 in studies, their infrequent occurrence hinders their broad application in urban settings. Pedestrians are

83 prevalent in urban areas, but their low image resolution and diminished presence in severely flooded zones

84 reduce their reliability and practicality as reference points for water level estimation.

85   Vehicles serve as ideal reference objects for recognizing urban flood levels, attributed to their stable

86 morphological features, widespread availability, and ease of detection. Current research leverages vehicles

87 for urban flood water level identification. For example, Park et al. (Park et al., 2021) and (Huang et al., 2020)

88 used Mask R-CNN to detect the submerged state of vehicles or their wheels as an indicator of flood levels.

89 (Huang et al., 2020; Park et al., 2021), while Wan et al. utilized the YOLO (You Only Look Once) series

90 models , a CNN-based computer vision (CV) model, for urban flood risk assessment and detection (Puliti

91 and Astrup, 2022; Redmon et al., 2016; Wan et al., 2024; Zhong et al., 2024). However, most studies use

92 cars as reference objects; yet, the diversity of car types (e.g., sedans, SUVs, and pickup trucks) introduces

93 significant variations in height and dimensions, affecting model generalization. Furthermore, the limited

94 height of car bodies means they cannot provide effective water level information once submerged up to the

95 roof, and their lower frequency of appearance in extreme weather makes it challenging to collect image

96 datasets.

97   In comparison, buses, as a critical component of urban transportation systems, possess standardized

98 heights and structures with minimal variation between models, making them a more ideal reference object

99 for flood water level monitoring. Buses overcome the limitations posed by cars, such as variations in size

100 and limited height. Additionally, buses primarily operate in busy or essential areas, and their ability to

101 withstand submersion is crucial for the continued operation of the urban public transportation system. Flood

102 level recognition based on the submerged status of buses can intelligently assess their water-related risks,

103 providing valuable support for urban transportation emergency management.

104   In response to the gaps in existing research, this study aims to create a comprehensive dataset of

105 submerged buses by sourcing flood images from social media platforms. Based on urban flood safety

106 standards and bus height characteristics, the submerged states of buses will be are categorized into specific

107 levels. The dataset includes complex scenes (e.g., nighttime, occlusions, and incomplete bus bodies) to

108 enhance data diversity.

109   YOLO is an efficient real-time object detection algorithm that simplifies the traditional multi-stage

110 detection pipeline by framing object detection as a regression problem. In the YOLO model, the image is

111 divided into a grid, with each grid cell predicting the location (bounding box) and class probability of an

112 object. The uniqueness of YOLO lies in its ability to predict multiple bounding boxes simultaneously in a

113 single forward pass, significantly improving computational efficiency and processing speed. The model

114 utilizes a convolutional neural network for feature extraction and considers the global context of the image,

115 which helps reduce the likelihood of false positives. The YOLOv8 algorithm, as the most recent iteration of

116 the YOLO series, has exhibited outstanding accuracy and rapid detection performance on the standard

117 COCO (Common Objects in Context) dataset (Wan et al., 2024). In this study, the YOLOv8 model is trained

118 on ~~a~~ the purpose-built dataset to improve its performance in identifying urban flood water levels with

119 precision.

120 This study introduces an innovative approach to flood level detection by leveraging the submerged

121 states of buses, addressing the limitations of traditional recognition methods based on cars and other

122 reference objects and overcoming the limitations of conventional monitoring techniques in broader

123 applications. Specifically, the objectives of this study include:

124 1) Developing a comprehensive dataset of submerged buses to examine the relationship between bus

125 submersion and flood water levels.

126 2) Evaluating the performance of YOLOv8 configurations in assessing flood severity through original and

127 augmented data training, as well as experiments involving complex scenes.

128 3) Proposing configuration recommendations for YOLOv8 aims to address diverse application scenarios,

129 ensuring efficient deployment in varied urban environments.

130 This paper is structured as follows: Section 2 provides a detailed description of the dataset construction,

131 data augmentation strategies, ~~and~~ YOLOv8 model configurations and~~,~~ explains the experimental design~~,~~ and

132 model evaluation metrics. Section 3 explains experimental results, followed by a comparative analysis of the

133 findings. Section 4 discusses the experimental results and offers configuration recommendations for

134 YOLOv8. Finally, Section 5 provides a summary of the main conclusions and highlights potential directions

135 for future research.

136 **2. Methodology**

137 **2.1 Data acquisition and processing**

138 **2.1.1 Data acquisition**

139 In this study, a comprehensive dataset of submerged buses was constructed, comprising 1,008 images

140 that capture buses in various statues of submersion. These submerged bus images were collected through

141 keyword searches such as urban flooding and submerged bus on Baidu and Google, screenshots of relevant

142 frames in short videos on Douyin, browsing urban flood news, and obtaining images from WeChat public

143 accounts. Due to the diverse sources of image data, the images ~~in exhibit differences~~ used in the experiment

144 vary in resolution and size. When selecting bus images, this study included complex and challenging scenes,

145 such as nighttime scenes, partial occlusions, and incomplete buses, to ensure the dataset's diversity. The

146 inclusion of these scenes may help enhance the diversity of the dataset, potentially enabling the trained model

147   to better handle various flood scenes.

148   All collected images of buses were manually screened to ensure that the depicted buses were either

149   stationary or normally moving through floodwater during flooding events, without signs of floating or water-

150   induced displacement. This process ensured the validity and reliability of buses as stable reference objects.

151   **2.1.2 Data annotation**

152   This study assesses flood risk levels based on the submersion status of buses. To ensure accurate

153   detection of the entire bus, four flood levels were defined, with detailed information on each flood level and

154   corresponding bus examples provided in Table 1. In this study, the approximate height of buses was

155   uniformly set to 3 meters in the model, based on the specifications of commonly observed urban bus types

156   in social media images. Based on a systematic evaluation of the images, it was found that the submersion

157   depths of buses were mostly concentrated between 0 and 50 cm, with values exceeding 100 cm observed

158   only in a few cases. Given that high water levels (greater than 100 cm) are relatively rare in urban scenarios,

159   this study chooses to define classification levels within the more commonly observed water depth range.

160   Consequently, four flood levels were established, with detailed information on each flood level and

161   corresponding bus examples provided in Table 1. Using Labelimg, a widely used annotation tool for object

162   detection model training, the 1,008 acquired images were annotated to identify 1,562 instances, which were

163   stored in YOLO format for subsequent training. Based on different states of bus movement, annotation types

164   were divided into two categories: holistic and segmented. In holistic annotation, the entire bus is assigned a

165   single flood level, while in segmented annotation, specific parts of the bus correspond to different levels, as

166   illustrated in Fig. 1.

167   **Table 1**

168   Flooded bus dataset: bus instances and flood levels.

Flood levels	Analysis of bus submersion depths	Range of water depth	Number of instances
Level1	bottom of wheels submerged; inner wheel contour not visible	0~20 cm	296
Level2	between bottom of wheels and halfway up the tires, between bottom of wheels and top edge of license plate, water reaches 1/4 of the step at bottom of door	20~45 cm	585
Level3	between halfway up the tires and full tire coverage, between top edge of license plate and bottom edge of windshield	45~100 cm	371
Level4	above the bottom edge of the windshield, fully submerged tires	>100 cm	310

169

(a) The entire bus is assigned a single flood level

(b) The specific part of bus is assigned different levels

Fig. 1. Examples of dataset annotations: (a) The entire bus is assigned a single flood level; (b) The specific part of bus is assigned different levels.

2.1.3 Data augmentation

The original dataset, comprising 1,008 images, is relatively small in scale, necessitating its enhancement and expansion to increase background complexity, prevent overfitting, and improve robustness. Image data augmentation methods can be broadly categorized into two types: luminosity distortions and geometric distortions(Li et al., 2023). The former involves adjusting image brightness, contrast, hue, saturation, and adding noise, while the latter encompasses random scaling, cropping, flipping, and rotation operations. In this study, horizontal and vertical flipping, rotation, and random cropping were applied to augment the original dataset, as illustrated in Fig. 2. All images in the augmented dataset were annotated using Labelimg and stored in YOLO format. Additionally, considering the potential for manual annotation bias, a review process was conducted to verify the correctness of all bounding boxes and annotations related to flood risk levels.
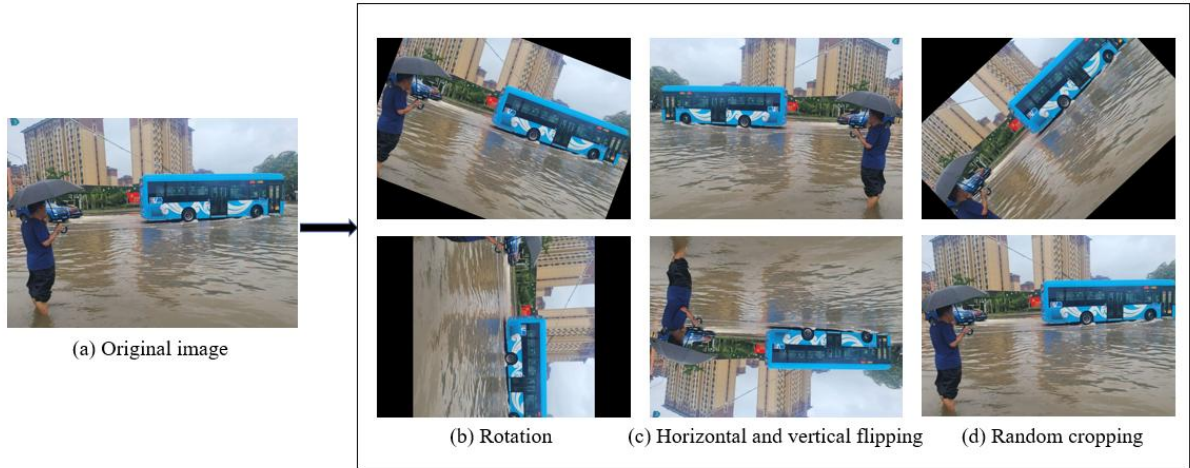
184
185 **Fig. 2.** Examples of dataset augmentations: (a) Original image; (b) Rotation; (c) Horizontal and vertical
186 flipping; (d) Random cropping.

187 **2.2 Object detection model**

188 A key feature of the YOLO model is its ability to achieve an optimal trade-off between speed and

189 accuracy, enabling rapid and precise object detection across a wide range of application scenes (Wan et al.,

190 2024). This study constructed an object detection model based on the YOLOv8 source code, which operates

191 on convolutional neural networks (CNN). YOLOv8 is an integrative and enhanced version building on

192 previous YOLO generations and represents the latest iteration in the YOLO series. This version significantly

193 improves computational efficiency and inference speed by optimizing the network architecture and refining

194 inference algorithms. Moreover, YOLOv8 demonstrates higher stability in multi-object detection tasks under

195 complex scenes, particularly with its advanced features such as automated hyperparameter tuning and

196 dynamic convolution modules. These enhancements further boost the model's flexibility and adaptability,

197 making it more capable of meeting the diverse requirements of real-world applications.

198 The YOLOv8 processing workflow includes image preprocessing, multi-level feature extraction

199 through CNN, and multi-scale feature fusion via a feature pyramid and path aggregation network. Following

200 this, adaptive anchor boxes are used for bounding box regression and classification prediction, with non-

201 maximum suppression applied to eliminate redundant bounding boxes. The model ultimately outputs the

202 target's class, bounding box, and confidence score, ensuring a balance between detection accuracy and

203 efficiency.

204 As shown in Fig. 3, the YOLOv8 network architecture is composed of three primary parts: Backbone,

205 Neck, and Head. The Backbone consists of five convolutional modules, four C2f modules, and ~~a SPPF~~a

206 Spatial Pyramid Pooling-Fast (SPPF) module, all designed for feature extraction. The Neck refines and

207 integrates features derived from the Backbone, improving both the precision and reliability of object

208 detection. The Head utilizes a decoupled structure to handle feature maps across multiple scales, generating

209 the final detection outputs.

210 (a) YOLOv8 network diagram   (d) C2f module architecture diagram
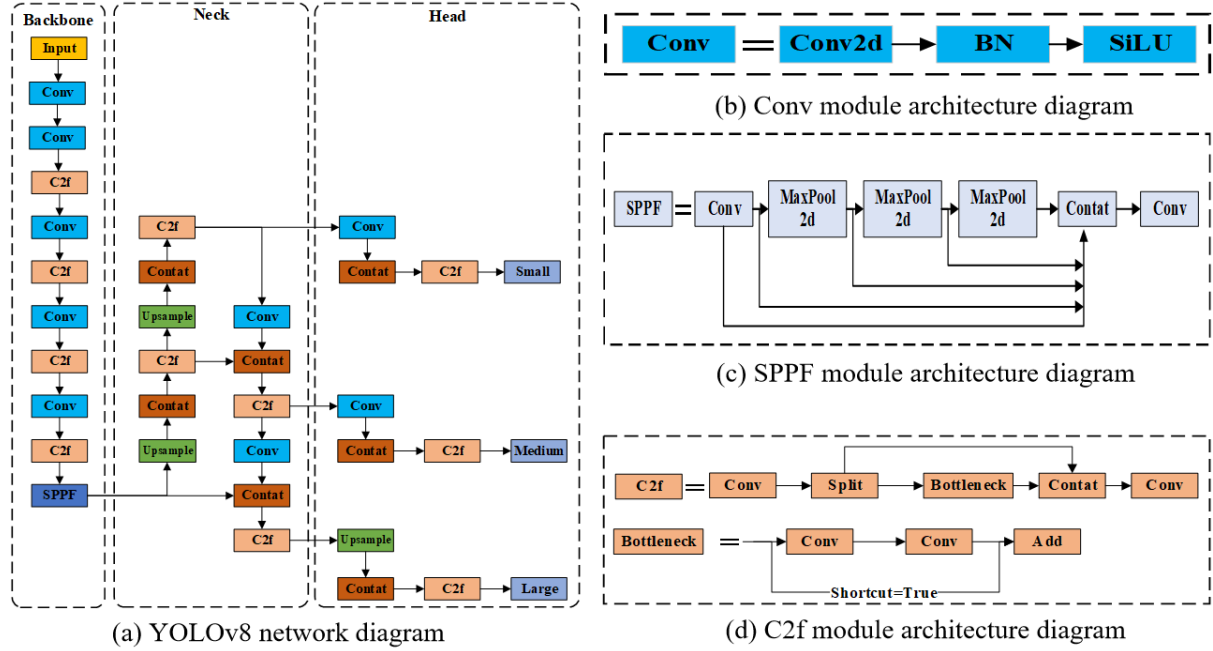
211 **Fig. 3.** The YOLOv8 network structure: (a) YOLOv8 network diagram; (b) Conv module architecture
212 diagram; (c) SPPF module architecture diagram; (d) C2f module architecture diagram.

213 **2.2.1 Experiment on object detection model**
214   Following data augmentation, the original dataset was expanded to 2,184 images for model training. In

215 this study, four different YOLOv8 configurations—YOLOv8n, YOLOv8s, YOLOv8m, and YOLOv8l—

216 were used for training, each designed with specific network depths and widths to address varying application

217 requirements. Table 2 presents the key characteristics of these four YOLOv8 configurations. The number of

218 layers reflects the depth of the model, with a greater number of layers indicating a deeper model capable of

219 capturing higher-level semantic features. However, this also leads to increased computational complexity.

220 Parameters refer to the total number of learnable weights and biases within the model. A higher number of

221 parameters signifies stronger representational capacity, making the model suitable for more complex tasks,

222 but it also requires greater computational resources and longer training times.

223 **Table 2**
224 The primary characteristics of the four YOLOv8 configurations.

Model	Size	Layers	Params (M)	mAP50-95on val (%)	FLOPs (B)	Speed CPU ONNX (ms)	Speed A100 TensorRT (ms)
YOLOv8n	640	225	3.2	37.3	8.7	80.4	0.99
YOLOv8s	640	225	11.2	44.9	28.6	128.4	1.20
YOLOv8m	640	295	25.9	50.2	78.9	234.7	1.83
YOLOv8l	640	365	43.7	52.9	165.2	375.2	2.39

2.2.2 Experimental setup

The model was implemented using PyTorch, a framework offering libraries for object detection models. Training was performed on NVIDIA Quadro RTX 3090 GPU. The original dataset contained 1,008 images, with 90% allocated for training and the remaining 10% for validation. The initial input size was set to 640 × 640, with a batch size of 16 and 100 training epochs. ~~In the data augmentation experiment, the augmented dataset expanded to 2,184 images, with 90% for training and 10% for validation, while all other settings remained the same as previously described.~~ In the data augmentation experiment, augmentation was applied only to the training set, resulting in 1,986 augmented training images. To maintain a consistent 90%-10% split ratio, the validation set was expanded from 108 to 198 images using non-augmented and previously unused images, while all other settings remained the same as previously described. Throughout the entire training process, the validation set was strictly separated from the training set, and the model had no access to any original or augmented images from the validation set. In this study, the official default hyperparameter settings of YOLOv8 were adopted.

2.2.3 Complex scenes prediction experiment

The performance of object detection models on the validation dataset does not fully represent its overall capabilities, as view of the bus, impacted by camera angle and distance, introduces numerous sources of interference. To address this, a complex scene prediction experiment was designed in this study to assess the detection capabilities of the different YOLOv8 configurations under challenging urban flood environments.

In this experiment, YOLOv8 models trained on either the original or augmented datasets were used to conduct complex scene predictions, evaluating their performance under challenging conditions. Fig. 4 presents two particularly demanding scenes, not in the existing dataset, Fig. 4a shows a rainy scene with multiple vehicles, where the incomplete view of the bus, impacted by camera angle and distance, introduces numerous sources of interference, increasing detection complexity. Fig. 4b depicts a nighttime scene of a submerged bus, where low light and poor image quality significantly elevate the difficulty of detection.
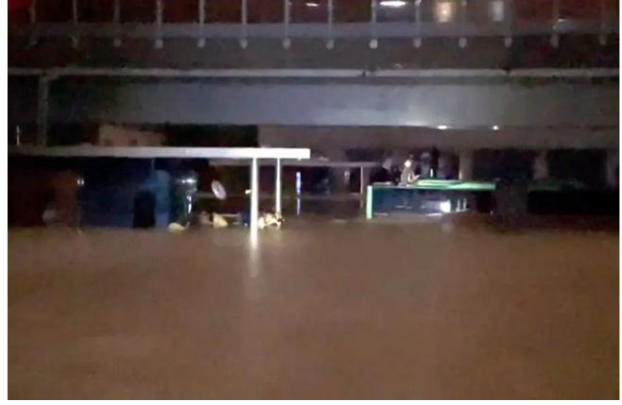
(a) Low flood risk scene with multiple vehicles present   (b) High flood risk scene with blurring and corruption

Fig. 4. Two complex urban flooding scenes: (a) Low flood risk scene with multiple vehicles present; (b) High flood risk scene with blurring and corruption.

2.2.4 Comparative experiment with YOLOv5 model

~~Although the introduction mentions that YOLOv8 is the latest algorithm in the YOLO series, a lack of comparative experimental data would be unconvincing.~~ Although the introduction states that YOLOv8 is the latest algorithm in the YOLO series, the absence of comparative experimental results with earlier YOLO versions weakens the argument for its superior performance. This study will compare and analyze the configuration demonstrating superior performance in the experiments with the corresponding configuration in the YOLOv5 model. The experiments include training on the original dataset, training with data augmentation, and complex scene prediction, following the same experimental setup described earlier.

2.3 Model evaluation

The widely recognized evaluation metrics, such as precision (P), recall (R), and F1 scores are as follows:

$$Precision = \frac{TP}{TP + FP} \tag{1}$$

$$Recall = \frac{TP}{TP + FN} \tag{2}$$

$$F1 = \frac{2 \times Precision \times Recall}{Precision + Recall} \tag{3}$$

Precision (P) quantifies the model's false detection rate, while Recall (R) evaluates its true detection rate. The F1-score evaluates model performance, particularly in object detection tasks, as it combines both P and R, representing their harmonic mean, where True Positive (TP) refers to the count of objects correctly identified as positive, True Negative (TN) denotes the count of non-objects accurately classified as negative, False Positive (FP) indicates the count of non-objects incorrectly classified as positive, and False Negative (FN) represents the count of objects wrongly classified as negative.

In this study, mean Average Precision (mAP), a well-established evaluation indicator, is utilized as the primary criterion to evaluate the performance of different YOLOv8 configurations in detecting bus submersion states. The mAP is computed by summing the average precision across all labels and dividing the result by the total number of categories. A higher mAP value signifies improved average accuracy of the model, indicating enhanced overall detection performance. The formula for calculating mAP is as follows:

$$mAP = \frac{1}{n}\sum_{i=1}^{n} AP_i = \frac{1}{n}\sum_{i=1}^{n} \int_0^1 P_i(R_i)dR_i \qquad (4)$$

where n is the number of categories, Average Precision (AP) is the area under the Precision–Recall (P–R) curve, P is used to measure the false detection rate of the model and R is used to measure the true detection rate, the formulas for P and R are given in Equations (1) and (2).

~~As the output quality of the model varies with changes in the Intersection over Union (IoU) threshold, it is standard practice to evaluate model performance across multiple IoU thresholds. IoU quantifies the overlap between the detection box (generated by the algorithm) and the ground truth box (annotated using labeling software), with a range of values from 0 to 1. A higher IoU value signifies better prediction accuracy, representing a greater overlap between the detection box and the ground truth box. The formula for calculating IoU is as follows:~~

Intersection over union (IoU) is a fundamental metric in object detection that measures the degree of overlap between the predicted bounding box (generated by the algorithm) and the ground truth bounding box (annotated using labeling software), with a range of values from 0 to 1. A higher IoU value signifies better prediction accuracy, representing a greater overlap between the predicted bounding box and the ground truth bounding box. The formula for calculating IoU is as follows:

$$IoU = \frac{A \cap B}{A \cup B} \qquad (5)$$

where A denotes the area of the detection box, while B refers to the area of the ground truth box.

mAP50 and mAP50-95 are core metrics for evaluating object detection model performance, each measuring the model's average detection precision under different IoU threshold conditions. mAP50 indicates the average precision computed at an IoU threshold of 0.5, where an overlap of over 50% between the detection box and ground truth box qualifies as a correct detection. This metric primarily reflects the model's basic object detection capability. mAP50-95, on the other hand, is the mean average precision

298 calculated across ten different IoU thresholds, from 0.5 to 0.95 in 0.05 increments. This metric averages AP

299 across multiple IoU thresholds, providing a comprehensive assessment of the model's performance. A higher

300 mAP50-95 value indicates stronger generalization ability across varying degrees of overlap within the same

301 scene. Collectively, mAP50 and mAP50-95 provide a thorough and objective evaluation of model prediction

302 accuracy and are extensively utilized in the domain of object detection.

303 **3. Result**

304 **3.1 Training experimental results**

305 **3.1.1 Analysis of training results on the original dataset**

306 This subsection provides a comparative evaluation of the training outcomes of the different YOLOv8

307 models on the original dataset. Each model was trained under the experimental settings outlined in Section

308 3.1. Fig. 5 illustrates the trend of mAP for each model during the training period, while Fig. 6 presents the

309 prediction performance of each model across individual classes.

310 As illustrated in Fig. 5a, following 100 epochs of training, the four models (YOLOv8n, YOLOv8s,

311 YOLOv8m, YOLOv8l) each reach convergence, achieving mAP50 values on the validation dataset of 0.618,

312 0.662, 0.611, and 0.639, respectively. YOLOv8s exhibits superior performance in this object detection task,

313 maintaining a higher mAP50 across the training duration compared to the other configurations. YOLOv8l

314 shows pronounced oscillations during the early training stages, requiring a longer stabilization period.

315 Furthermore, it is observable that mAP50 for all models increases rapidly in the early epochs (0-20), after

316 which the growth rate decelerates and plateaus. Notably, an increase in network width (param) and depth

317 (layer) for YOLOv8 does not yield a substantial improvement in mAP50.

(a) The trend of mAP50   (b) The trend of mAP50-95
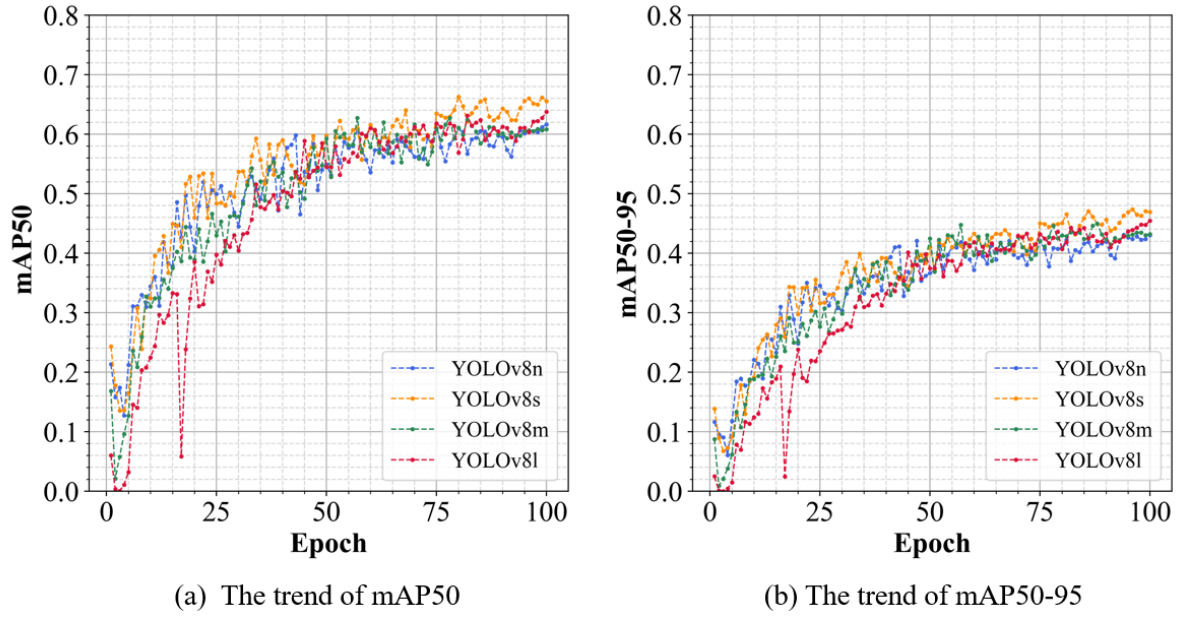
Fig. 5. The mAP of the validation dataset throughout the training process (a) The trend of mAP50; (b) The trend of mAP50-95.

As shown in Fig. 6, the detection performance of the four YOLOv8 models varies across different flood risk levels. The YOLOv8s model demonstrates superior average precision across all flood risk categories, with an mAP50 of 0.662. For low flood risk category identification (level 1), all models achieve satisfactory detection results. However, for higher flood risk categories, the detection performance of YOLOv8n, YOLOv8m, and YOLOv8l is below expectations, with only YOLOv8s effectively capturing the submersion characteristics of buses at high water levels, thereby achieving relatively accurate identification. Although the YOLOv8l model has higher complexity and a larger parameter scale, its AP values for the level 3 and level 4 categories are 0.591 and 0.530, respectively, significantly lower than those of the YOLOv8s model, which are 0.632 and 0.602. This suggests that, for detecting high flood risk features, increased model complexity does not inherently result in improved detection accuracy.
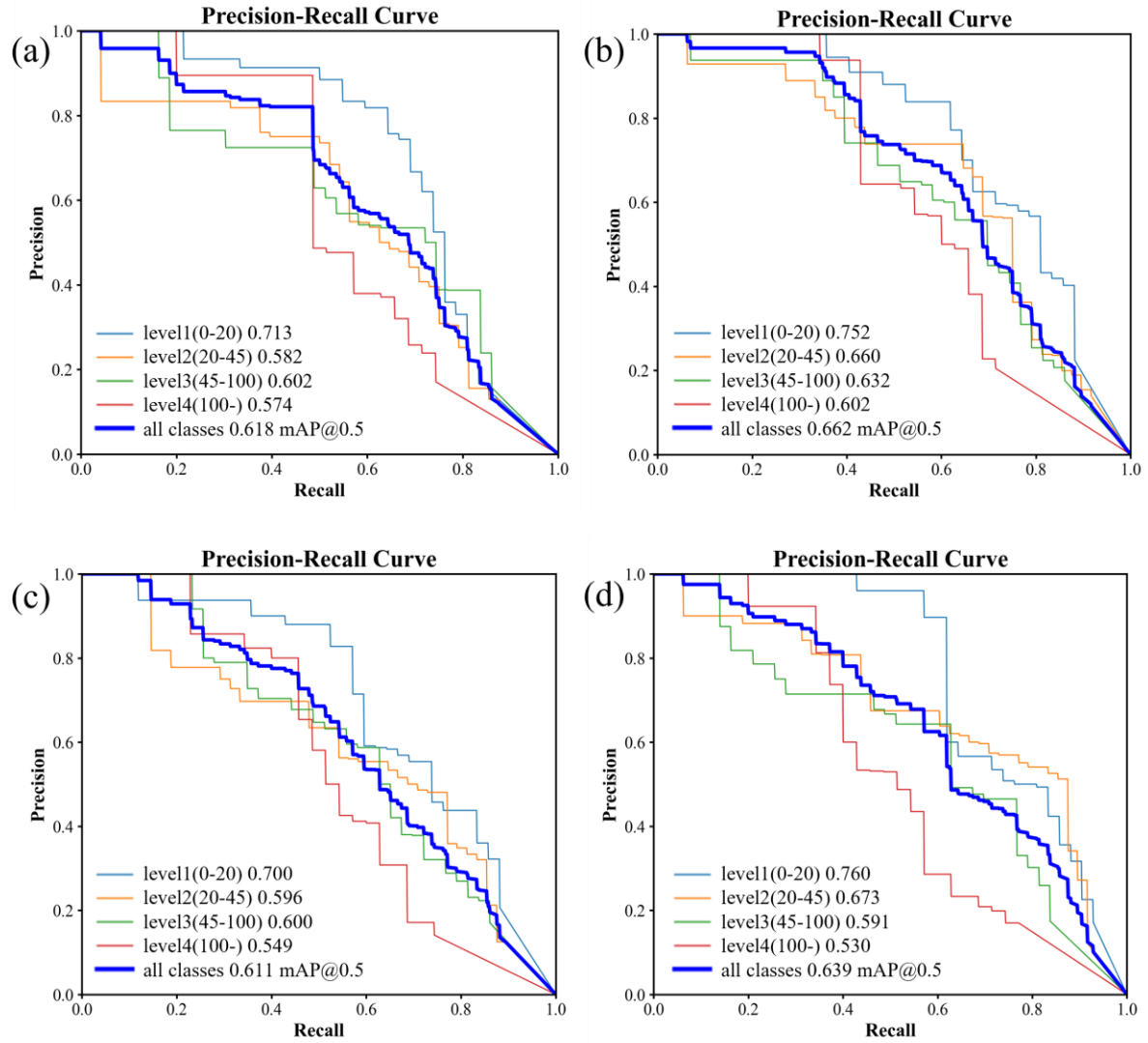
331
332 **Fig. 6.** Precision-recall curve for each class of validation process: (a) YOLOv8n Validation Results; (b)
333 YOLOv8s Validation Results; (c) YOLOv8m Validation Results; (d) YOLOv8l Validation Results.

3.1.2 Analysis of training results on the augmented dataset

335   This subsection ~~provides a comparative evaluation of the training outcomes of the different~~ compares

336 the training performance of different YOLOv8 models on the augmented dataset. Fig. 7 illustrates the mAP

337 trend, while Fig. 8 presents the prediction performance of each model.

338   As depicted in Fig. 7a, after 100 training epochs, the four models (YOLOv8n, YOLOv8s, YOLOv8m,

339 YOLOv8l) ~~each~~ all converge, reaching mAP50 values on the validation dataset of 0.722, 0.734, 0.716, and

340 0.703, respectively. ~~Data augmentation has yielded substantial improvements in both mAP50 and mAP50-~~

341 ~~95 for all models, which will be analyzed in further detail in the next subsection.~~ Among them, ~~Following~~

342 ~~augmentation,~~ YOLOv8s consistently outperforms the other models~~., with a higher mAP50 value.~~ The early-

343 stage fluctuations observed during YOLOv8l training disappear, resulting in smoother curves and a more

344 stable optimization process. ~~After incorporating data augmentation, the initial jump phenomenon observed~~

345 ~~during YOLOv8l training disappears, resulting in smoother curves and a more stable optimization process~~.

346 However, compared to other models, the performance improvement of YOLOv8l during the early stages of

347 training remains relatively slower. This may be attributed to the model's higher complexity and larger

348 parameter scale.

(a) The trend of mAP50   (b) The trend of mAP50-95
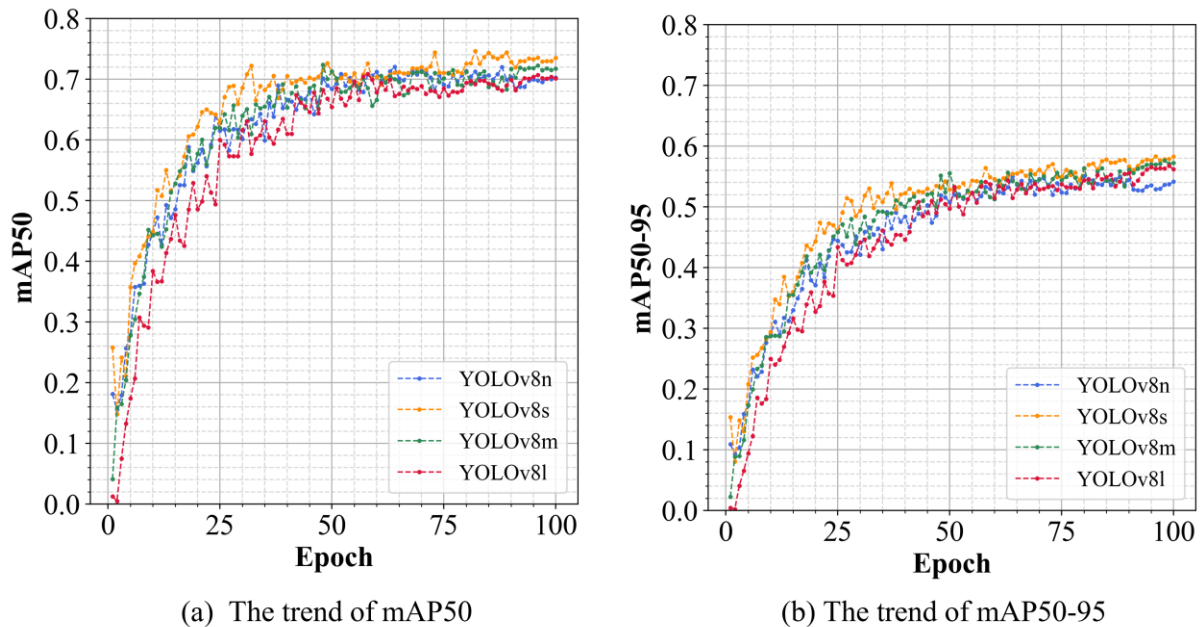
349
350 **Fig. 7.** The mAP of the validation dataset throughout the training process after data augmentation: (a) The
351 trend of mAP50; (b) The trend of mAP50-95.

352 As illustrated in Fig. 8, following data augmentation, the four YOLOv8 models exhibit similar

353 performance in detecting each flood risk level. The highest overall effectiveness is found in YOLOv8s,

354 achieving an mAP50 of 0.734, with consistently high precision and recall across all flood risk categories.

355 ~~Post-augmentation, all~~ All models effectively capture the submersion characteristics of buses at various

356 water levels, with AP values for each category exceeding 0.67, indicating robust performance on the

357 validation dataset.

358 Notably~~Moreover~~, the detection results for higher-risk categories (Level 3 and Level 4) show improved

359 AP values in all models,~~data augmentation significantly improved the detection capabilities of all models~~

360 ~~for higher-level categories (Level 3 and Level 4),~~ as evidenced by the Precision-Recall curves shifting closer

361 to the upper-right corner. For example, in the YOLOv8n model, the AP value for Level 3 increased from

362 0.602 to 0.712, and for Level 4, from 0.574 to 0.746. Similarly, in the YOLOv8l model, the AP value for

363 Level 3 rose from 0.600 to 0.685, and for Level 4, from 0.549 to 0.679. This improvement is primarily

364 attributed to enhanced data diversity,~~Data augmentation enhanced the diversity of training samples,~~

365 effectively mitigating the interference caused by variations in viewpoint and object scale. This not only

366 improved the model's ability to detect higher-level targets but also enhanced the overall detection

367 performance.
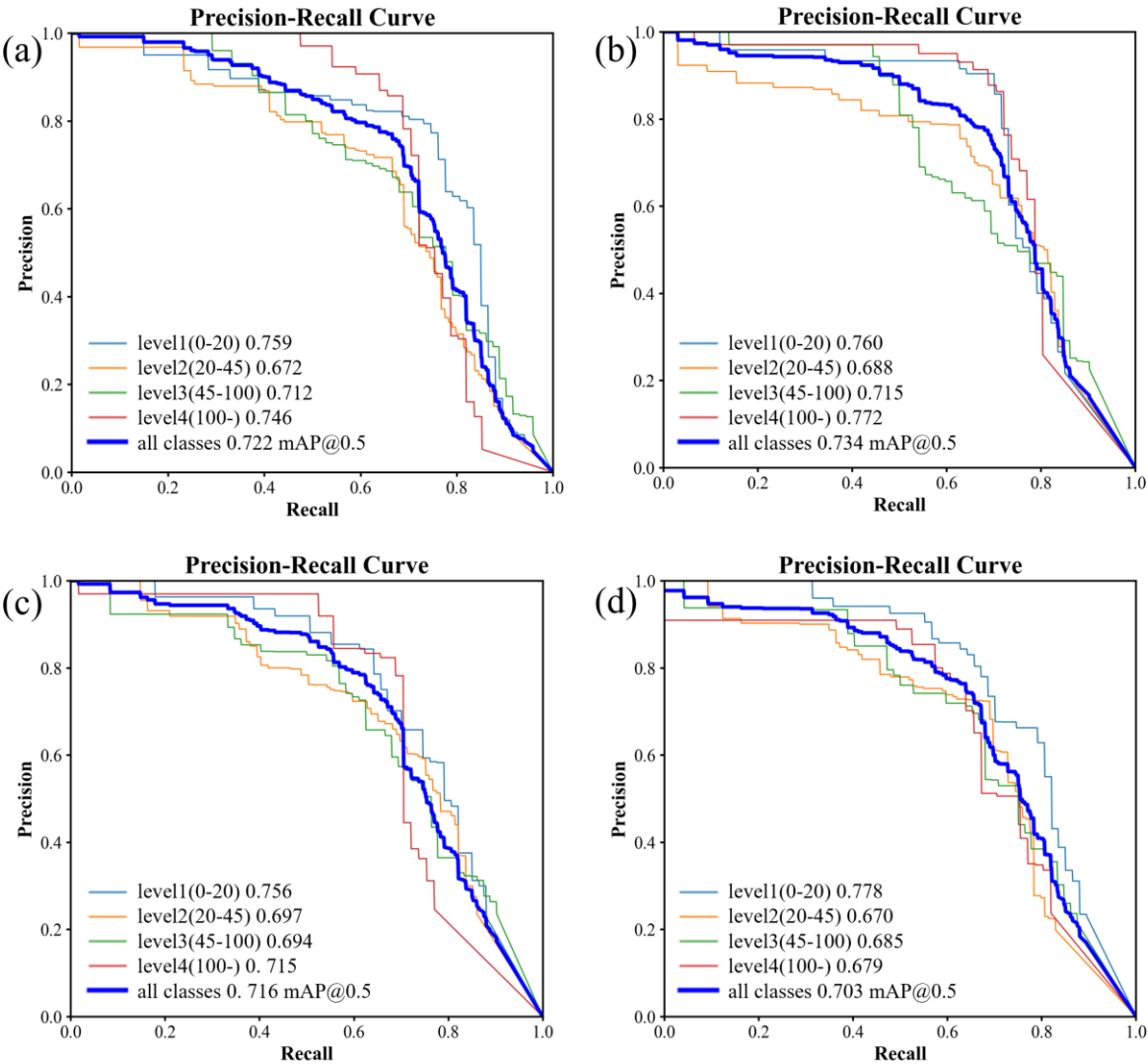
368
369 **Fig. 8.** Precision-recall curve for each class of validation process after data augmentation: (a) YOLOv8n
370 Validation Results; (b) YOLOv8s Validation Results; (c) YOLOv8m Validation Results; (d) YOLOv8l
371 Validation Results.
372   This study provides a comparative analysis of the detection performance of different YOLOv8 model

373 configurations before and after data augmentation. Table 3 presents the mAP50, mAP50-95, and training

374 times for the optimal YOLOv8 models

375 **Table 3**
376 mAP and training time for four YOLOv8 configurations: pre- and post-data augmentation.

YOLO v8	mAP50 (%)			mAP50-95 (%)			training time (h)	
	original dataset	augmented dataset	increase	original dataset	augmented dataset	increase	original dataset	augmented dataset
n	61.7	72.2	17.0	43.0	55.2	28.4	0.102	0.325
s	66.0	73.4	11.2	47.5	58.2	22.5	0.152	0.483
m	61.2	71.6	17.0	45.0	57.4	27.6	0.293	0.930
l	63.8	70.3	12.2	45.4	56.6	24.7	0.438	1.390

377   As indicated in Table 3, data augmentation led to significant enhancements in model detection

378 performance, with substantial increases in both mAP50 and mAP50-95 across all configurations. For mAP50,

379 all models demonstrated improvements exceeding 10%, while mAP50-95 gains surpassed 20% for each

380 configuration. YOLOv8m and YOLOv8n exhibited the highest mAP50 increases, whereas YOLOv8s

381 showed the smallest gain at 11.2%. In terms of mAP50-95, YOLOv8n achieved the greatest improvement,

382 rising from 43.0% to 55.2% (28.4% increase), while YOLOv8s displayed the smallest increase at 22.5%.

383 In terms of overall performance, YOLOv8s achieved the highest mAP50 and mAP50-95 values across

384 all configurations, reaching 73.4% and 58.2%, respectively, with a moderate training time. By contrast,

385 YOLOv8l achieved similar mAP50 and mAP50-95 values but required nearly triple the training time.

386 Similarly, YOLOv8m showed performance close to that of YOLOv8s, though with a nearly doubled training

387 time.

3.2 Experimental results in complex scenes

3.2.1 Validation results of models on the original dataset

390 This section presents a comparative evaluation of the validation outcomes for the four optimized

391 YOLOv8 models trained on the original dataset. The numbers in the top-right corner of the detection boxes

392 (ranging from 0 to 1) represent the confidence level of the model for the detection results. ~~The numbers on~~

393 ~~the image represent the confidence level of the model for the detection results.~~ As shown in Fig. 9, all four

394 models can detect the flood risk level of the bus. However, only YOLOv8l correctly identifies it as level 1,

395 albeit with low confidence, while the other models incorrectly classify it as level 2. At low flood risk levels,

396 none of the models effectively capture the critical distinguishing features, highlighting limitations in their

397 generalization capabilities.

(a) Detection outcomes obtained using YOLOv8n (b) Detection outcomes obtained using YOLOv8s
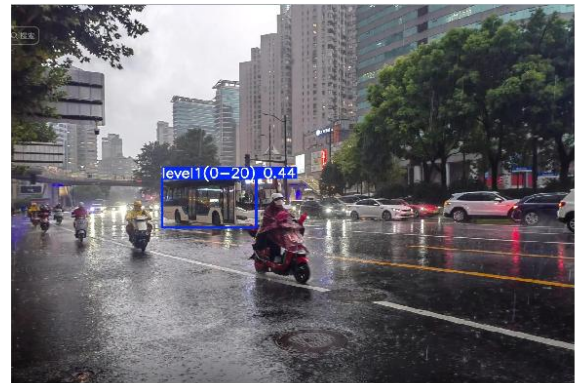
(c) Detection outcomes obtained using YOLOv8m (d) Detection outcomes obtained using YOLOv8l

Fig. 9. Comparison of YOLOv8 detection results in low flood risk scene with multiple vehicles present (pre-augmentation): (a) Detection outcomes obtained using YOLOv8n; (b) Detection outcomes obtained using YOLOv8s; (c) Detection outcomes obtained using YOLOv8m; (d) Detection outcomes obtained using YOLOv8l.

Moreover, Fig. 10 presents the validation results at a high flood risk level. All four optimal YOLOv8 models successfully detect the blurred bus in the image and identify its submerged state with high confidence. For the bus located at the upper-right edge of the image, none of the models detected it due to low lighting, though they were able to make partial level assessments. The models have learned to extract key features associated with incomplete bus bodies from the dataset. Furthermore, YOLOv8l incorrectly classified the bus station and surrounding environment as level 4 submersion.

| (a) Detection outcomes obtained using YOLOv8n | (b) Detection outcomes obtained using YOLOv8s |

(c) Detection outcomes obtained using YOLOv8m   (d) Detection outcomes obtained using YOLOv8l

Fig. 10. Comparison of YOLOv8 detection results in high flood risk scene with blurring and corruption (pre-augmentation): (a) Detection outcomes obtained using YOLOv8n; (b) Detection outcomes obtained using YOLOv8s; (c) Detection outcomes obtained using YOLOv8m; (d) Detection outcomes obtained using YOLOv8l.

3.2.2 Validation results of models on the augmented dataset

This section provides a comparative evaluation of the validation outcomes for the four optimized YOLOv8 models after data augmentation. As shown in Fig. 11, all four models accurately detect the flood risk level of the bus with high confidence. In this detection, the best performance is found inYOLOv8n, exhibiting higher confidence levels than the other models. Besides, both YOLOv8s and YOLOv8m unexpectedly generated a level 2 prediction box during bus detection.
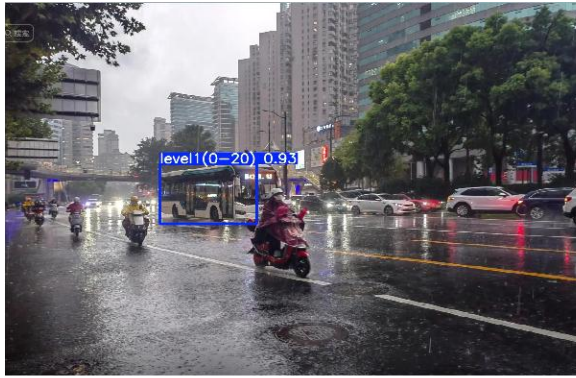
(a) Detection outcomes obtained using YOLOv8n   (b) Detection outcomes obtained using YOLOv8s
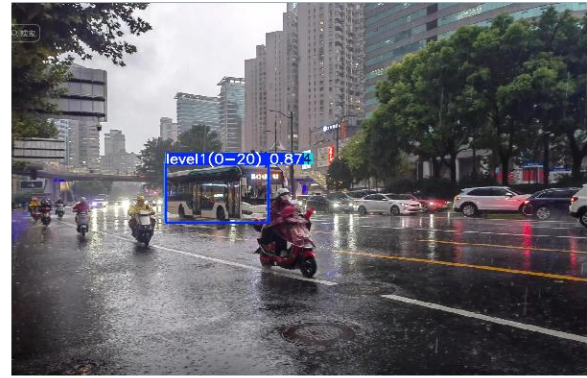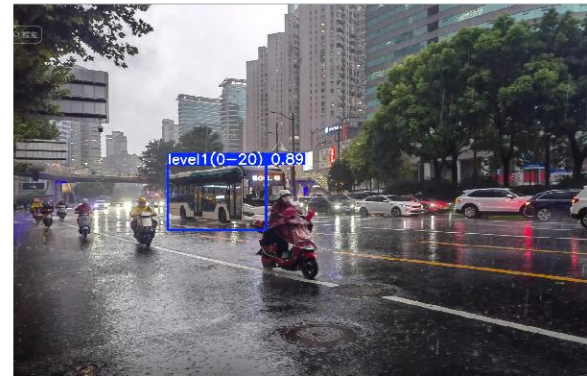
(c) Detection outcomes obtained using YOLOv8m   (d) Detection outcomes obtained using YOLOv8l

Fig. 11. Comparison of YOLOv8 detection results in low flood risk scene with multiple vehicles present (post-augmentation): (a) Detection outcomes obtained using YOLOv8n; (b) Detection outcomes obtained using YOLOv8s; (c) Detection outcomes obtained using YOLOv8m; (d) Detection outcomes obtained using YOLOv8l.

Fig. 12 presents the validation results at a high flood risk level. All four optimal YOLOv8 models successfully detect the blurred bus in the image, accurately identifying its submerged state with high confidence. The highest confidence is found in YOLOv8s, without any false detections. However, none of the models detected the bus body located at the upper-right edge of the image, even after data augmentation. Besides, YOLOv8m and YOLOv8l incorrectly classified the bus station and background environment as level 4 submersion.

In summary, data augmentation resulted in notable improvements in both recognition accuracy and confidence across the four optimal models, enhancing their ability to accurately detect bus submersion states. In addition, detection performance under low-light conditions remains an area requiring further refinement.

(a) Detection outcomes obtained using YOLOv8n (b) Detection outcomes obtained using YOLOv8s

(c) Detection outcomes obtained using YOLOv8m (d) Detection outcomes obtained using YOLOv8l

Fig. 12. Comparison of YOLOv8 detection results in high flood risk scene with blurring and corruption (pre-augmentation): (a) Detection outcomes obtained using YOLOv8n; (b) Detection outcomes obtained using YOLOv8s; (c) Detection outcomes obtained using YOLOv8m; (d) Detection outcomes obtained using YOLOv8l.

3.3 Experimental results compared with YOLOv5

3.3.1 Analysis of training experiment results

Fig. 13 displays the precision-recall curves from the training results. A comparison reveals that YOLOv8s outperforms YOLOv5s on both the original and augmented datasets, indicating that YOLOv8s achieves higher detection accuracy in image recognition tasks. On the original dataset, YOLOv5s attains an mAP50 of 0.555, while YOLOv8s reaches 0.662, reflecting a performance gap of 19.3%. After data augmentation, although the performance gap between YOLOv5s and YOLOv8s narrows, YOLOv8s continues to lead. Additionally, results from the two training experiments with YOLOv5 indicate that data augmentation has a substantial impact on enhancing the training effectiveness of YOLO models
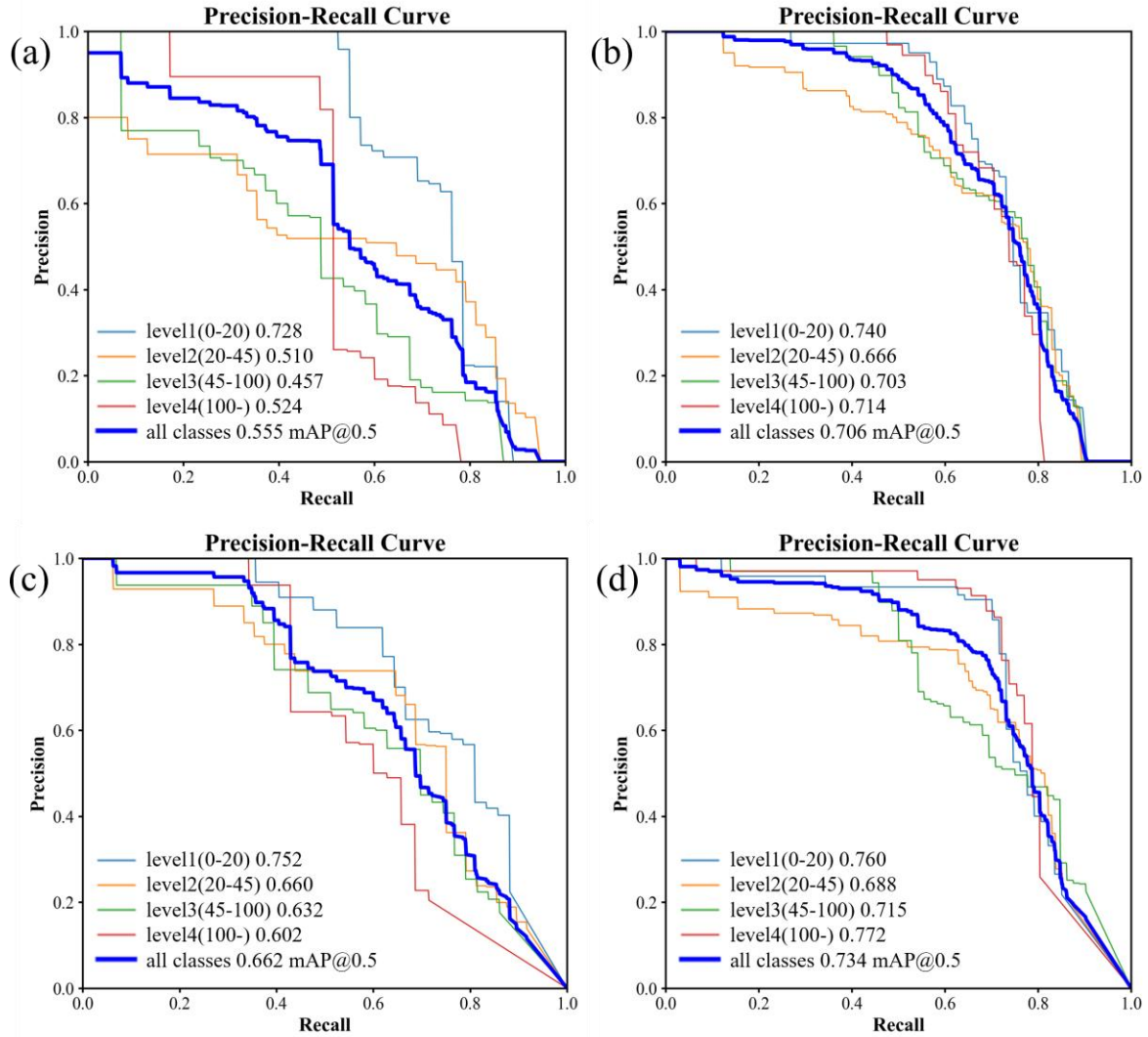
449
450 **Fig. 13.** Precision-recall curves from the training results: (a) YOLOv5s validation results on original dataset;
451 (b) YOLOv5s validation results on augmented dataset; (c) YOLOv8s validation results on original dataset;
452 (d) YOLOv8s validation results on augmented dataset.

453 **3.3.2 Analysis of scene prediction experiment results**
454   This section evaluates the stability and effectiveness of YOLOv5s and YOLOv8s under challenging

455 conditions by testing their performance in two complex urban scenes. Fig. 14 and Fig. 15 illustrate the

456 detection results of YOLOv5s and YOLOv8s in low and high flood risk scenes, respectively. In the low-risk

457 scene, YOLOv5s accurately identifies the bus and correctly predicts its submersion status, similar to

458 YOLOv8s; however, the confidence level of YOLOv5s, even after data augmentation, shows limited

459 improvement. YOLOv8s, on the other hand, demonstrates higher detection confidence and accuracy

460 following data augmentation. In the high-risk scene, characterized by blurred or partially degraded images,

461 YOLOv5s performs notably well. YOLOv5s detects targets that YOLOv8s fails to recognize, likely due to

462 its capacity for handling noisy data. This difference in performance under extreme conditions suggests that

463 the network structure of YOLOv5s may enhance detection in low-quality images, offering insights for

464   potential optimizations in YOLOv8s.

(a) YOLOv5s detection results on original dataset   (b) YOLOv5s detection results on augmented dataset

(c) YOLOv8s detection results on original dataset   (d) YOLOv8s detection results on augmented dataset

465
466   **Fig. 14.** Comparison of YOLO detection results in low flood risk scene with multiple vehicles present: (a)
467   YOLOv5s detection results on original dataset; (b) YOLOv5s detection results on augmented dataset; (c)
468   YOLOv8s detection results on original dataset; (d) YOLOv8s detection results on augmented dataset.
469
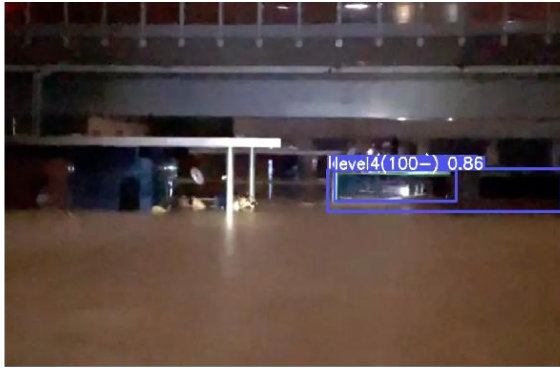
(a) YOLOv5s detection results on original dataset   (b) YOLOv5s detection results on augmented dataset

(c) YOLOv8s detection results on original dataset   (d) YOLOv8s detection results on augmented dataset

Fig. 15. Comparison of YOLO detection results in high flood risk scene with blurring and corruption: (a) YOLOv5s detection results on original dataset; (b) YOLOv5s detection results on augmented dataset; (c) YOLOv8s detection results on original dataset; (d) YOLOv8s detection results on augmented dataset.

4. Discussion

4.1 Impact of data augmentation

The dataset size plays a critical role in determining the performance of YOLOv8 models. The object detection experiment results in Section 3.1 demonstrate the positive effect of data augmentation on model performance. Models trained with the augmented dataset achieved substantial improvements, with mAP50 and mAP50-95 on the validation set increasing by over 10% and 20%, across all YOLOv8 configurations. This indicates that data augmentation significantly enhances detection accuracy while improving model stability and generalization across various IoU thresholds.

The impact of data augmentation on performance varies across different YOLOv8 models. YOLOv8n, the configuration with the fewest parameters, demonstrates the largest performance gain post-augmentation, with the most substantial increases in both mAP50 and mAP50-95. In contrast, YOLOv8s, which performed well on the original dataset, exhibits the smallest performance improvement after augmentation. This suggests that YOLOv8s is already highly effective at extracting key features of detection targets, even with a relatively small dataset. Although the performance gain for YOLOv8s is minimal, it consistently delivers

The data augmentation strategy significantly enhanced model performance in complex scene experiments. Prior to augmentation, all four YOLOv8 models may exhibited false detections and low confidence levels under challenging conditions such as low light at night, blurred imagery, and partial occlusions. Post-augmentation, however, each YOLOv8 model showed notable improvements in detection accuracy and confidence in complex scenes. For instance, in multi-vehicle environments, the augmented YOLOv8 models were able to accurately detect the submersion status of buses with high confidence, whereas pre-augmentation models failed to make correct identifications. These findings indicate that data augmentation plays a crucial role in enhancing model recognition capabilities under complex conditions, enabling more robust performance in the variable environments encountered in practical applications. The enhancement in model performance achieved through the data augmentation strategy stems from the YOLOv8 model's robust learning and generalization capabilities. By increasing data diversity through augmentation techniques such as rotation, flipping, and random cropping, the model is compelled to extract the critical features of detection targets with greater precision. Additionally, the expanded dataset after augmentation provides a larger volume of annotated instances, enriching the training samples from which the model can learn. This enhanced dataset supports more robust feature extraction, contributing to overall performance gains.

4.1 Impact of dataset size and diversity

The size and diversity of the training dataset play a critical role in determining the performance of YOLOv8 models. Models trained with the augmented dataset achieved substantial improvements, with mAP50 and mAP50-95 on the validation set increasing by over 10% and 20% (Table 3), across all YOLOv8 configurations. This improvement can be credited to the enhanced learning and generalization abilities of models. The increased number and diversity of training samples not only enable a more comprehensive understanding of the key features of detection targets but also allow for a broader representation of annotated instances, enhancing the model's ability to learn. Such exposure to varied input scenarios equips YOLOv8 with enhanced generalization, leading to better results in the validation stage.

Moreover, this benefit extends beyond training to inference capabilities. Under challenging conditions such as low illumination, motion blur, and partial occlusion, models trained on the augmented dataset

exhibited greater robustness, reflected in higher detection confidence. Dataset diversity is therefore key to

improving training performance and significantly enhancing inference in complex real-world environments.

The impact of dataset size and diversity varies across different YOLOv8 configurations. YOLOv8n, with the smallest number of parameters, is particularly responsive to changes in training sample volume, showing the most notable improvement in mAP when trained on the augmented dataset. In contrast, YOLOv8s, which already performed well on the original dataset, shows the smallest relative gain. Nevertheless, it consistently delivers the best results across multiple experiments.

4.2 Impact of detection target

In previous studies, cars have commonly been used for flood detection (Puliti and Astrup, 2022; Redmon et al., 2016; Wan et al., 2024; Zhong et al., 2024) . However, the diversity in car models limits annotation standardization and reduces the model's generalization capability. Additionally, the relatively low height of cars constrains their effectiveness as reliable flood detection references. For instance, in Wan et al.'s study on complex scenes (Wan et al., 2024) , only sedans were successfully identified, while pickup trucks in the images were challenging to detect. In contrast, buses offer standardized body structures, greater urban coverage, and consistent height characteristics, making them a more promising reference object for flood detection. The experiments and validations in this study demonstrate the strong performance of the object detection model trained on bus images, with its PR curve closely approaching the upper-right corner. The best model achieved an mAP50 of 0.734 across all categories on the test dataset, surpassing the previous study result of mAP50 at 0.707 (Wan et al., 2024). Moreover, since buses predominantly operate in busy or critical areas, their ability to withstand water directly impacts the stability of urban public transportation systems. The bus submersion-based detection approach developed in this study effectively enhances flood risk assessment accuracy, providing a more scientific basis for future urban flood monitoring and emergency management.

4.3 2 Recommended configurations for YOLOv8

Based on the comprehensive performance of different YOLOv8 configurations during training and in complex scenes, this study recommends prioritizing the YOLOv8s model for urban flood detection using bus imagery. Although the YOLOv8l model theoretically offers higher network complexity and parameter count, which should enable more granular feature extraction, its performance improvements in this

experiment were not significant. In contrast, the YOLOv8s model demonstrated superior results across multiple performance metrics and achieved an effective balance between model accuracy, training time, and computational resource requirements. Therefore, in environments with limited resources and high computational costs, YOLOv8s has proven to be the most advantageous choice.

When computational resources and dataset availability are ample, YOLOv8m or YOLOv8l should be considered as priority options. As dataset size expands and more computational resources become available, the performance potential of YOLOv8m and YOLOv8l models may be more fully realized. With larger datasets, the deeper network structures and advanced feature extraction capabilities of YOLOv8m and YOLOv8l can better capture critical features and details of the targets, resulting in higher accuracy and stability in object detection.

4.3 Advantages and disadvantages

Crowdsourced images from social media have emerged as a high-value data source for acquiring flood information (Huang et al., 2020). The YOLO object detection model requires annotated images as input for training, and such annotation can be performed by non-experts, making the method highly scalable. Buses, as structurally standardized and dimensionally stable vehicles, provide reliable and scalable reference objects for flood status identification. Moreover, buses typically operate in traffic-intensive or critical urban areas, where water-related safety concerns directly impact the stability of the public transportation system. The bus submergence detection technique adopted in this study significantly enhances the precision of urban flood risk assessment, offering a more scientific basis for future flood monitoring and emergency response in cities.

Compared with existing studies, the method proposed in this paper demonstrates distinct advantages in terms of reference object selection and object detection algorithms. The present study can be compared with these approaches as follows: (Jiang et al., 2020), (Bhola et al., 2018) and (Alizadeh Kharazi and Behzadan, 2021) respectively utilized traffic cones and guardrails, bridge structures, and sign poles as reference indicators. Although these objects offer advantages such as fixed structure and known physical dimensions, their applicability is often confined to specific locations with fixed viewing angles and clearly visible reference targets, and they are usually deployed only in limited areas. In contrast, this study adopts buses as reference objects. Given their extensive operating routes and easily recognizable structural features, the proposed method enables flood perception across broader urban road networks, thereby exhibiting enhanced

572 spatiotemporal adaptability.

573 (Huang et al., 2020) and (Park et al., 2021) applied the Mask R-CNN model to detect vehicle tires or

574 body structures to support flood level estimation. While their methods achieve high prediction accuracy,

575 Mask R-CNN is a two-stage detection framework with a complex architecture and relatively slow inference

576 speed. Additionally, it is highly sensitive to image quality and susceptible to errors under occlusion, water

577 splashes, or reflection interference—conditions common in real-world flood scenarios—which limits its

578 real-time applicability and environmental robustness (Huang et al., 2020). By contrast, the YOLOv8 model

579 adopted in this study is a single-stage, end-to-end detection framework. It demonstrates superior robustness

580 and detection speed under complex scene conditions and can stably identify reference targets, reducing false

581 detection rates. Its lightweight architecture also facilitates deployment on edge devices, making it suitable

582 for practical engineering applications.

583 (Wan et al., 2024) employed YOLOv8 to classify flood submergence levels of cars and achieved the

584 highest mAP50 of 0.707, demonstrating satisfactory detection accuracy. In their complex scenario testing,

585 sedans could be correctly identified, whereas pickup trucks failed to be recognized. This observation

586 indicates that the diversity of vehicle features may affect the model's generalization capability. In

587 comparison, the structural consistency and height stability of buses help reduce the impact of target

588 variability on model performance. Moreover, the best-performing model in this study achieved a mAP50 of

589 0.734, demonstrating superior detection accuracy.

590 This study demonstrates that floodwater levels in urban areas can be effectively identified by detecting

591 the submergence status of buses using the YOLOv8 model. The proposed method has been validated in

592 terms of feasibility and practical potential. However, further research is warranted to enhance the model's

593 adaptability and applicability. On the one hand, the current dataset remains limited in scale, with insufficient

594 images under nighttime or low-light conditions, which constrains the model's performance under such

595 scenarios. Future work may incorporate illumination-guided transformers or light-aware attention

596 mechanisms to improve model robustness under challenging lighting environments. Simultaneously,

597 expanding the data acquisition scope and incorporating more diverse scenes will be critical for improving

598 detection accuracy. On the other hand, the current detection framework does not support quantitative

599 estimation of floodwater depth. Future research could explore regression-based modules that leverage the

600 actual height of buses and the geometric relationships within images to develop numerically interpretable

601 flood level estimators, thereby providing more actionable support for urban emergency response and flood

602 risk management.

5. Conclusions

604 This study proposes an urban flood detection method based on the YOLOv8 deep learning model, which

605 accurately assesses flood risk levels by identifying the submersion state of buses. A dataset of 1,008 images

606 depicting submerged buses was collected from online platforms and expanded to 2,184 images using data

607 augmentation strategies. Subsequently, the submersion states of buses were annotated into four levels for

608 training the object detection model. Finally, the performance of various YOLOv8 models was compared

609 through data augmentation and complex scene validation experiments, resulting in the following

610 experimental insights:

611 1) The highest detection accuracy for flood risk levels is achieved by YOLOv8s. Although YOLOv8m

612 and YOLOv8l demonstrated comparable overall performance, they required significantly greater

613 computational resources and training time.

614 2) The application of data augmentation significantly enhanced the detection accuracy and robustness of

615 the YOLOv8 models, improving their recognition precision and generalization capabilities when

616 confronted with complex scenes.

617 2) The use of buses as reference objects for flood detection presents notable advantages, including high

618 consistency and standardized structure, overcoming the limitations of previous reference objects such

619 as cars, thereby making them more suitable for urban flood detection.Compared with commonly used

620 reference objects in existing studies, buses offer advantages such as structural standardization,

621 consistent height, and wide spatial coverage, making them more suitable for flood identification at the

622 urban scale.

623 3) This study offers configuration recommendations for YOLOv8 models tailored to urban flood

624 detection based on the submersion state of buses.

625 This study supplements and extends existing research on flood detection by validating the feasibility

626 and effectiveness of using buses as reference objects for the identification of urban flood risk levels. This

627 study explores the application potential of bus submersion state detection within the YOLOv8 framework.

628 This approach broadens the technical pathways for urban flood monitoring and provides crucial support for

629   flood emergency management within urban transportation systems, demonstrating practical value in the field

630   of disaster prevention and mitigation.

631   This study primarily relies on social media image recognition to determine flood risk levels. However,

632   the model's performance remains limited in certain complex scenes, such as those involving extreme lighting

633   conditions. Additionally, the model currently lacks the capability to quantitatively measure flood depth,

634   which is critical for precise flood risk assessment. Future research will concentrate on devising methods for

635   quantitative flood depth estimation using bus submersion states and creating noise-resistant model

636   architectures to improve the model's applicability and precision.

637   **Data availability:**

638   Data will be made available on request.

639   **Declaration of competing interest**

640   The authors declare that they have no known competing financial interests or personal

641   relationships that could have appeared to influence the work reported in this paper.

642   **Computer Code Availability:**

643   The code in this study can be obtained from the Git repository:

644   https://github.com/ydkyly/dataset_and_result.git.

645   **Authorship Statement**

646   **Yanbin Qiu:** Writing – original draft, Validation, Software, Methodology, Investigation. **Xudong Zhou:**
647   Writing – review & editing, Validation. **Jiaquan Wan:** Writing – review & editing, Project administration,
648   Validation. **Tao Yang:** Writing – review & editing, Supervision. **Lvfei Zhang:** Formal analysis, Validation.
649   **Yuanzhuo Zhong:** Data curation, Validation. **Leqi Shen:** Data curation, Validation. **Xinwu Ji:** Validation.

650

651 **References**

652 Alizadeh Kharazi, B. and Behzadan, A. H.: Flood depth mapping in street photos with image processing and
653 deep neural networks, Comput. Environ. Urban Syst., 88, 101628,
654 https://doi.org/10.1016/j.compenvurbsys.2021.101628, 2021.

655 Baranowski, D. B., Flatau, M. K., Flatau, P. J., Karnawati, D., Barabasz, K., Labuz, M., Latos, B., Schmidt,
656 J. M., Paski, J. A. I., and Marzuki: Social-media and newspaper reports reveal large-scale meteorological
657 drivers of floods on Sumatra, Nat. Commun., 11, 2503, https://doi.org/10.1038/s41467-020-16171-2, 2020.

658 Betterle, A. and Salamon, P.: Water depth estimate and flood extent enhancement for satellite-based
659 inundation maps, Nat. Hazards Earth Syst. Sci., 24, 2817–2836, https://doi.org/10.5194/nhess-24-2817-2024,
660 2024.

661 Bhola, P. K., Nair, B. B., Leandro, J., Rao, S. N., and Disse, M.: Flood inundation forecasts using validation
662 data generated with the assistance of computer vision, J. Hydroinformatics, 21, 240–256,
663 https://doi.org/10.2166/hydro.2018.044, 2018.

664 Chaudhary, P., D'Aronco, S., Leitão, J. P., Schindler, K., and Wegner, J. D.: Water level prediction from
665 social media images with a multi-task ranking approach, ISPRS J. Photogramm. Remote Sens., 167, 252–
666 262, https://doi.org/10.1016/j.isprsjprs.2020.07.003, 2020.

667 DeVries, B.: Rapid and robust monitoring of flood events using Sentinel-1 and Landsat data on the Google
668 Earth Engine, Remote Sens. Environ., 2020.

669 Fohringer, J., Dransch, D., Kreibich, H., and Schröter, K.: Social media as an information source for rapid
670 flood inundation mapping, Nat. Hazards Earth Syst. Sci., 15, 2725–2738, https://doi.org/10.5194/nhess-15-
671 2725-2015, 2015.

672 Guan, Y., Zheng, F., Zhang, P., and Qin, C.: Spatial and temporal changes of meteorological disasters in
673 China during 1950–2013, Nat. Hazards, 75, 2607–2623, https://doi.org/10.1007/s11069-014-1446-3, 2015.

674 Huang, J., Kang, J., Wang, H., Wang, Z., and Qiu, T.: A Novel Approach to Measuring Urban Waterlogging
675 Depth from Images Based on Mask Region-Based Convolutional Neural Network, Sustainability, 12, 2149,
676 https://doi.org/10.3390/su12052149, 2020.

677 Iqbal, U., Perez, P., Li, W., and Barthelemy, J.: How computer vision can facilitate flood management: A
678 systematic review, Int. J. Disaster Risk Reduct., 53, 102030, https://doi.org/10.1016/j.ijdrr.2020.102030,
679 2021.

680 Jafari, N. H., Li, X., Chen, Q., Le, C.-Y., Betzer, L. P., and Liang, Y.: Real-time water level monitoring
681 using live cameras and computer vision techniques, Comput. Geosci., 147, 104642,
682 https://doi.org/10.1016/j.cageo.2020.104642, 2021.

683 Jiang, J., Liu, J., Cheng, C., Huang, J., and Xue, A.: Automatic Estimation of Urban Waterlogging Depths
684 from Video Images Based on Ubiquitous Reference Objects, Remote Sens., 11, 587,
685 https://doi.org/10.3390/rs11050587, 2019.

686 Jiang, J., Qin, C.-Z., Yu, J., Cheng, C., Liu, J., and Huang, J.: Obtaining Urban Waterlogging Depths from
687 Video Images Using Synthetic Image Data, Remote Sens., 12, 1014, https://doi.org/10.3390/rs12061014,
688 2020.

689 Kankanamge, N., Yigitcanlar, T., Goonetilleke, A., and Kamruzzaman, Md.: Determining disaster severity
690 through social media analysis: Testing the methodology with South East Queensland Flood tweets, Int. J.
691 Disaster Risk Reduct., 42, 101360, https://doi.org/10.1016/j.ijdrr.2019.101360, 2020.

692 Kramer, M., Terheiden, K., and Wieprecht, S.: Safety criteria for the trafficability of inundated roads in
693 urban floodings, Int. J. Disaster Risk Reduct., 17, 77–84, https://doi.org/10.1016/j.ijdrr.2016.04.003, 2016.

694 Kundu, S., Lakshmi, V., and Torres, R.: Flood Depth Estimation during Hurricane Harvey Using Sentinel-
695 1 and UAVSAR Data, Remote Sens., 14, 1450, https://doi.org/10.3390/rs14061450, 2022.

696 Li, J., Cai, R., Tan, Y., Zhou, H., Sadick, A.-M., Shou, W., and Wang, X.: Automatic detection of actual
697 water depth of urban floods from social media images, Measurement, 216, 112891,
698 https://doi.org/10.1016/j.measurement.2023.112891, 2023.

699 Liang, J.: A local thresholding approach to flood water delineation using Sentinel-1 SAR imagery, ISPRS J.
700 Photogramm. Remote Sens., 2020.

701 Nayak, S. and Zlatanova, S.: Remote sensing and GIS technologies for monitoring and prediction of disasters,
702 Springer, Berlin London, 2008.

703 Park, S., Baek, F., Sohn, J., and Kim, H.: Computer Vision–Based Estimation of Flood Depth in Flooded-
704 Vehicle Images, J. Comput. Civ. Eng., 35, 04020072, https://doi.org/10.1061/(ASCE)CP.1943-
705 5487.0000956, 2021.

706 Paul, J. D., Buytaert, W., and Sah, N.: A Technical Evaluation of Lidar-Based Measurement of River Water
707 Levels, Water Resour. Res., 56, e2019WR026810, https://doi.org/10.1029/2019WR026810, 2020.

708 Pregnolato, M., Ford, A., Wilkinson, S. M., and Dawson, R. J.: The impact of flooding on road transport: A
709 depth-disruption function, Transp. Res. Part Transp. Environ., 55, 67–81,
710 https://doi.org/10.1016/j.trd.2017.06.020, 2017.

711 Puliti, S. and Astrup, R.: Automatic detection of snow breakage at single tree level using YOLOv5 applied
712 to UAV imagery, Int. J. Appl. Earth Obs. Geoinformation, 112, 102946,
713 https://doi.org/10.1016/j.jag.2022.102946, 2022.

714 Qian, Y., Chakraborty, T. C., Li, J., Li, D., He, C., Sarangi, C., Chen, F., Yang, X., and Leung, L. R.:
715 Urbanization Impact on Regional Climate and Extreme Weather: Current Understanding, Uncertainties, and
716 Future Research Directions, Adv. Atmospheric Sci., 39, 819–860, https://doi.org/10.1007/s00376-021-1371-
717 9, 2022.

718 Redmon, J., Divvala, S., Girshick, R., and Farhadi, A.: You Only Look Once: Unified, Real-Time Object
719 Detection, in: 2016 IEEE Conference on Computer Vision and Pattern Recognition (CVPR), 2016 IEEE
720 Conference on Computer Vision and Pattern Recognition (CVPR), Las Vegas, NV, USA, 779–788,
721 https://doi.org/10.1109/CVPR.2016.91, 2016.

722 Rosser, J. F., Leibovici, D. G., and Jackson, M. J.: Rapid flood inundation mapping using social media,
723 remote sensing and topographic data, Nat. Hazards, 87, 103–120, https://doi.org/10.1007/s11069-017-2755-
724 0, 2017.

725 Smith, L., Liang, Q., James, P., and Lin, W.: Assessing the utility of social media as a data source for flood
726 risk management using a real-time modelling framework, J. Flood Risk Manag., 10, 370–380,
727 https://doi.org/10.1111/jfr3.12154, 2017.

728 Voulodimos, A., Doulamis, N., Doulamis, A., and Protopapadakis, E.: Deep Learning for Computer Vision:
729 A Brief Review, Comput. Intell. Neurosci., 2018, 1–13, https://doi.org/10.1155/2018/7068349, 2018.

730 Wan, J., Qin, Y., Shen, Y., Yang, T., Yan, X., Zhang, S., Yang, G., Xue, F., and Wang, Q. J.: Automatic
731 detection of urban flood level with YOLOv8 using flooded vehicle dataset, J. Hydrol., 639, 131625,
732 https://doi.org/10.1016/j.jhydrol.2024.131625, 2024.

733 Yang, Z. and Wang, Q.: MINING METHOD OF TRAFFIC IMPACT AREAS OF RAINSTORM EVENT
734 BASED ON SOCIAL MEDIA IN ZHENGZHOU CITY, Int. Arch. Photogramm. Remote Sens. Spat. Inf.
735 Sci., XLVIII-3/W1-2022, 79–86, https://doi.org/10.5194/isprs-archives-XLVIII-3-W1-2022-79-2022, 2022.

736   Zhong, P., Liu, Y., Zheng, H., and Zhao, J.: Detection of Urban Flood Inundation from Traffic Images Using
737   Deep Learning Methods, Water Resour. Manag., 38, 287–301, https://doi.org/10.1007/s11269-023-03669-
738   9, 2024.